Solid-State Electronics 200 (2023) 108525

Contents lists available at ScienceDirect

Solid State Electronics

journal homepage: www.elsevier.com/locate/sse

Deriving a novel methodology for nano-BioFETs and analysing the effect of high-k oxides on the amino-acids sensing application

Rakshita Dhar [a,*], Naveen Kumar [a], Cesar Pascual Garcia [b], Vihar Georgiev [a]

[a] Device Modelling Group, James Watt School of Engineering, University of Glasgow, UK
[b] Nano-Enabled Medicine and Cosmetics Group, Materials Research and Technology Department, Luxembourg Institute of Science and Technology (LIST), Belvaux, Luxembourg

ARTICLE INFO

The review of this paper was arranged by "Francisco Gamiz"

Keywords:
ISFET
Nano-biosensing
MATLAB simulation
Functionalization
Analytical simulations

ABSTRACT

In this paper, we present simulation results of a BioFET using methodology based on the Gouy-Chapman-Stern and the Site-binding models. The derived simulation approach is used to sense different amino acids, such as Arginine (R), Aspartic Acid (D) and Proline (P), functionalized with the help of a linker connected to the gate-oxide. The performance of the BioFETs is optimized while analyzing the effect of high-k dielectrics as the gate oxide. In general, the channel oxides are responsible for tuning the parameters such as sensitivity, surface potential and intrinsic buffer capacity. The variation of total surface capacitance, the second derivative of drain current and surface potential are used to uniquely identify the signatures of different amino acids. The proposed method can be helpful in defining an efficient method for label-free protein sequencing.

1. Introduction

Since 1952, when Shockley invented Field-Effect Transistors (FETs), there have been undergoing many significant modifications to cater to the needs of sensing applications [1]. In 1970, Bergveld developed an ion-sensitive Field-Effect Transistor (ISFET) that is used for ion detection in a chemical environment [2]. With further development of technology and its application for biosensing, novel functionalized ISFET devices have been fabricated for protein and DNA detection [3 4]. Various simulation methodologies and fabrication techniques have been carried out to further expand the knowledge of the impact of sensor surface functionalization on the device performance [5 6].

In this paper, we have adopted a design-of-experiment approach based on an analytical model. The analytical model is implemented in a MATLAB simulation environment and it effectively combines the Gouy-Chapman-Stern model with the Site-binding model, which allows us to simulate various amino acids (AAs) immobilized on different high-k dielectrics as gate oxides [7 8]. Three AAs with different side chains are chosen to show the effect of high-k dielectric functionalization on the device sensitivity. The chosen AAs are Arginine (R), Aspartic Acid (D) and Proline (P). The high-k oxides used are titanium oxide (TiO_2), hafnium oxide (HfO_2) and silicon dioxide (SiO_2). The Gouy-Chapman-Stern layer model combines the Helmholtz and the diffuse double layer of the Gouy-Chapman model to explain the development of the double-layer capacitance on the sensor's surface [9]. The Site-binding model is used to describe the surface charge developed at the oxide/electrolyte interface [8]. This paper presents a new methodology that combines these two theories and our new method is applied to AAs immobilized on the sensor surface. Moreover, our simulation work shows that each AA has a unique signature (fingerprints) that can be used to distinguish and identify each AA [10].

Fig. 1 shows the schematic diagram of the BioFET implemented in the simulations. As an example, D is immobilized over the linker with a carboxylic terminal which eliminates the affinity corresponding to the C- terminal. Similarly, the chosen AAs can be immobilized by either carboxylic or amine terminal leaving the AA with lower affinity sites. The surface potential (Ψ_0) is calculated assuming the point charges that are separated from the oxide surface by the length and the effective permittivity of the AAs. Our simulation approach allows us to calculate Ψ_0, the sensitivity factor (α), the intrinsic buffer capacity (β) and the zeta potential (Ψ_ξ) for different oxides [7]. From this, we can also calculate the depletion width (W_D), the drain current (I_{SD}) and the 2nd order derivative of I_{SD} for each immobilized AAs (R, D and P). More importantly, all of these characteristics can be used as unique fingerprints for

* Corresponding author.
E-mail addresses: r.dhar.1@research.gla.ac.uk (R. Dhar), naveen.kumar@glasgow.ac.uk (N. Kumar), cesar.pascual@list.lu (C.P. Garcia), vihar.georgiev@glasgow.ac.uk (V. Georgiev).

https://doi.org/10.1016/j.sse.2022.108525

Available online 14 November 2022

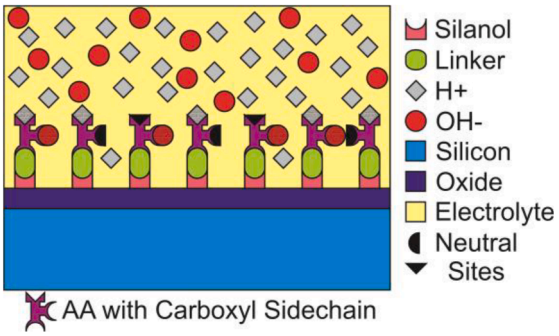

Fig. 1. Schematic diagram of the BioFET sensor with immobilised amino acids over the oxide. AA denotes the amino acid with carboxyl sidechains (example-Aspartic Acid). At the very bottom, the light blue colour is the Silicon nanowire channel. Immediately on top of it, as seen in purple colour, is the oxide that can be TiO_2, HfO_2 or SiO_2. The Silanol groups (SiOH) are represented directly above that as will be the case when SiO_2 is an oxide. The top of a silanol group is covered with light green colour which is the linker also known as a polyethylene glycol (PEG) layer. PEG is covalently bonded to amino acid on one side and to silanol on the other. The AA has the possibility to be protonated/deprotonated or to have active sites (for the receptors to attach).

the identification of AAs and polypeptides.

2. Methodology

For each gate oxide and immobilized AAs, we calculated first the surface charge density (σ_i) (with i = 1 to 5 depending on the AA radicals) using the site-binding model for the three C or N terminals immobilized AAs that we calculated in this work: C-Imm. D [σ_1], C-Imm. R [σ_2], C-Imm. P [σ_3], N-Imm. D [σ_4], N-Imm. R [σ_1] and N-Imm. P [σ_5] where

$$\sigma_1 = qN_S\left(\frac{cH_s^2 - K_aK_b}{K_aK_b + K_bcH_S + cH_S^2}\right) \tag{1}$$

$$\sigma_2 = qN_S\left(\frac{cH_s^2 + cH_SK_a}{K_aK_b + K_bcH_S + cH_S^2}\right) \tag{2}$$

$$\sigma_3 = qN_S\left(\frac{cH_S}{cH_S + K_a}\right) \tag{3}$$

$$\sigma_4 = qN_S\left(\frac{-cH_SK_a - K_aK_b}{K_aK_b + K_bcH_S + cH_S^2}\right) \tag{4}$$

$$\sigma_5 = qN_S\left(\frac{-K_a}{cH_S + K_a}\right) \tag{5}$$

and, $cH_s = cH_B exp\frac{-\Psi_0}{2V_T}$, $cH_B = 10^{-pH_B}$, $V_T = \frac{K_BT}{q}$, cH_s & cH_B represents the surface and bulk proton concentration respectively, pH_B is the bulk pH, N_S is the total surface states, K_a & K_b are the dissociation constants of the corresponding reactive sites of each AA and V_T is the thermal voltage. σ_i is equated and calculated iteratively with the σ_{DL} (surface charge density of Gouy-Chapman stern layer model) until the error < tolerance (10^{-50}). Bi-section method is adopted to find the point-of-zero charge (pH_{pzc}) [isoelectric point] and zeta potential (Ψ_ξ) for a particular surface charge density. Ψ_ξ is then subsequently used to find the Ψ_0, which includes the potential drop across the stern layer (Ψ_{Stern}) and is given by the following relation:

$$\Psi_0 = \Psi_{Stern} + \Psi_\xi = \frac{Q_0\sinh(\Psi_\xi/V_T)}{C_{stern}} + \Psi_\xi \tag{6}$$

where C_{Stern} is the capacitance of the stern layer. C_{Stern} is considered to be $0.8F/m^2$ [11]. Using Ψ_0, sensitivity factor (α), intrinsic buffer capacity (β) and 2nd order derivative of surface potential $\left(\frac{\partial^2\Psi_0}{\partial pH^2}\right)$ can be calculated as shown below [12].

$$\alpha = \frac{1}{1 + 2.303\frac{k_B\,T\,C_{diff}}{q^2\beta}} \tag{7}$$

$$\frac{\delta\sigma_{DL}}{\delta pH_S} = -q\beta \tag{8}$$

$$\frac{\partial^2\psi_0}{\partial pH^2} = -2.3\frac{kT.\partial\alpha}{q.\partial pH_B} \tag{9}$$

A high-aspect-ratio junctionless p-type FinFET structure is used for current simulations as it gives a larger surface area for the target molecules to come in contact with the receptors [13]. The depletion width (W_D) and drain current (I_{SD}) calculations are done as mentioned in ref. [14,15]. This occurs while solving the continuity equation across the electrolyte-oxide–semiconductor interfaces, using Ψ_0 as the variable parameter.

3. Results and discussions

Fig. 2(a) shows the variation of zeta potential (Ψ_ξ) with respect to pH_B. The point-of-zero-charge (pH_{pzc}) for SiO_2, HfO_2 and TiO_2 can be seen as the pH at which the Ψ_ξ crosses the zero value. Table 1 shows the summary of pH_{pzc}. Ψ_ξ is the potential between the stern potential and the shear plane which is most negative for the SiO_2 due to its higher affinity for losing protons and Ψ_ξ is most positive for HfO_2 because of its higher pK value of protonated sites. For SiO_2, the pH_{pzc} is in agreement with the experimental value. In the case of HfO_2 and TiO_2, the pH_{pzc} simulation value differs from the data available in the literature. This may be attributed to the ways in which oxides are grown and impurities present on the surface of oxides [18].

As shown in Fig. 2(b), α is minimum at pH_{pzc} for all three oxides. For HfO_2, pH_{pzc} is around 7, which is higher than SiO_2 and TiO_2, since the change in Ψ_ξ with respect to pH_B is higher for enhanced sensitivity. The increment in α is observed for all gate oxides before and after pH_{pzc} as this is due to the increase in Ψ_ξ away from the pH_{pzc}. β has a similar trend with respect to pH_B as it denotes the change in surface charge density (σ_0) with respect to surface pH (pH_S) as shown in Fig. 2(c). Fig. 3(a) shows the Ψ_0 variation with respect to pH for all three gate oxides. This follows the Ψ_ξ with the addition of Ψ_{Stern} as per equation 6. Non-linearity of Ψ_0 for TiO_2 is due to the large difference between the affinity constants [16]. Fig. 3(b) is the 2nd order derivative of Ψ_o with respect to pH_B that shows the transition of reactive sites over the oxide from protonation to deprotonation clarifying the pH_{pzc} value. Fig. 3(c) shows the total capacitance (C_T) that consists of C_{stern}, double-layer capacitance (C_{DL}) and intrinsic AA capacitance (C_{AA}), where all of them are connected in series with each other as shown below.

$$\frac{1}{C_T} = \frac{1}{C_{stern}} + \frac{1}{C_{DL}} + \frac{1}{C_{AA}} \tag{10}$$

TiO_2 shows better resolution for ion-sensing with higher total capacitance (C_T) as compared to the other two oxides, SiO_2 and HfO_2. As the last step, we consider SiO_2 and TiO_2 as an oxide surface for the immobilization of the three different AAs (R, D and P). Two variants of each AA are considered - C-Imm. and N-Imm. (carboxylic or amine terminal is immobilized respectively). The full surface coverage (no active silanol active groups on the surface) by the AA is considered for simulation. Fig. 4(a) and 5(a) show the depletion width (W_D) variation with respect to pH_B for different AAs immobilized over the SiO_2 and TiO_2 as gate oxide respectively. Considering the FET to be completely depleted at the lowest pH, a shift in potential towards negative decreases the depletion width. With the same depletion width at the lowest pH, the higher permittivity of TiO_2 amplified the effect of Ψ_0 to further decrease the depletion width as compared to the SiO_2. Fig. 4(b) and 5(b) represent the drain current (I_{SD}) variation with respect to the pH_B for SiO_2 and

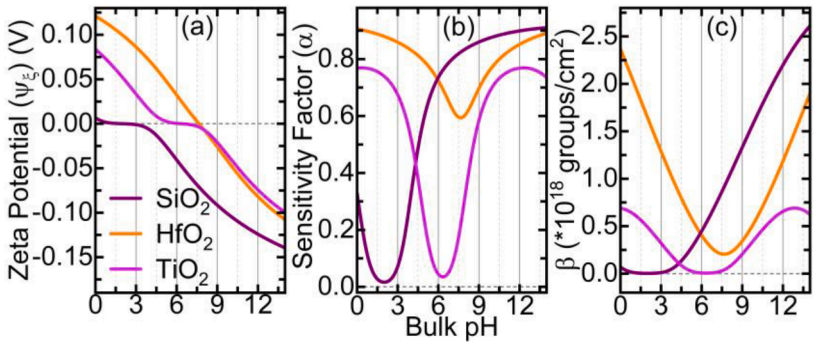

Fig. 2. (a) Zeta potential (Ψ_ξ), (b) sensitivity factor (α) and (c) intrinsic buffer capacity (β) variation in relation to pH for three different gate oxide materials.

Table 1
Values of $pH_{pzc(sim)}$ for the three different oxides obtained from simulation results vs points of zero charge taken from literature for the three oxides ($pH_{pzc(lit)}$).

Gate Oxide	$pH_{pzc(sim)}$	$pH_{pzc(lit)}$
SiO_2	2	2 [7]
HfO_2	7.65	7.4 [16]
TiO_2	6.33	6.7 [17]

TiO_2 respectively. As the depletion width increases in a pMOS, the I_{SD} decreases and vice versa. From both graphs, it can be observed that the TiO_2 helped in distinguishing the difference in current to identify the AAs. This can be attributed to the dissociation constants and the oxide capacitance. Figs. 4(c) and 5(c) show the BioFET behavior with immobilized AAs in terms of $\frac{\partial^2 I_{SD}}{\partial pH^2}$. Indeed, each AA shows very unique behavior of the isoelectric and inflection points which can be used as unique fingerprints to identify each AA. C-Imm. R and P exhibit positive charges on the oxide surface across the pH range due to the presence of only amine sites. The positive charge acquired by C-Imm. R is more than C-Imm. P due to an extra amine sidechain. C-Imm. D is more balanced due to the presence of C-terminal sidechain and N-terminal with an isoelectric point at pH = 6.625. N-Imm. D and P result in negative charges over the surface across the pH range due to the presence of only carboxylic sites with an extra sidechain in N-Imm. D. whereas, N-Imm. R is balanced with an isoelectric point at pH = 7.325 similar to the C-Imm. D. Figs. 4(c) and 5(c) represent the 2nd order derivative of I_{SD} $\left(\frac{\partial^2 I_{SD}}{\partial pH^2}\right)$ for SiO_2 and TiO_2 respectively in presence of AA which varies depending on the affinities of reactive sites. Different site-binding relations are used to calculate the Ψ_0. The affinity of the remaining amine/ carboxyl sites and sidechains is responsible for the distinct fingerprints of the AAs in the

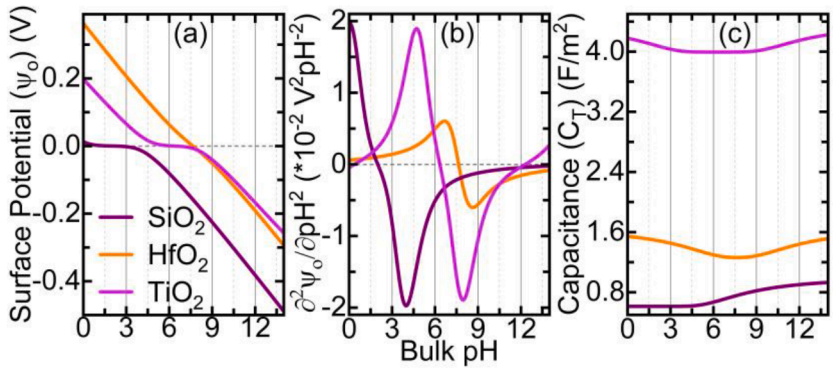

Fig. 3. (a) Surface potential (Ψ_0), (b) 2nd order derivative of Ψ_0 $\left(\frac{\partial^2 \Psi_0}{\partial pH^2}\right)$ and (c) total capacitance (C_T) vs pH. Graphs shown three different gate oxide materials.

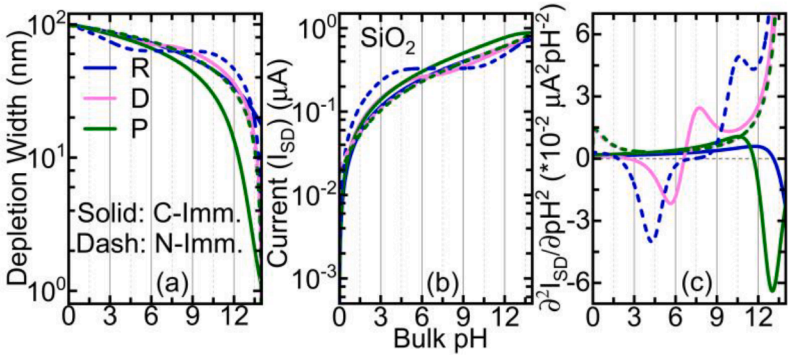

Fig. 4. (a) Depletion width (W_D) (b) drain current (I_{SD}) and (c) 2nd order derivative of I_{SD} $\left(\frac{\partial^2 I_{SD}}{\partial pH^2}\right)$ vs pH. Graphs shown are for Arginine (R), Aspartic Acid (D) & Proline (P) amino acids considering SiO_2 as a gate oxide with carboxyl group immobilised (solid line: C-Imm) and amine group immobilised (dash line: N-Imm).

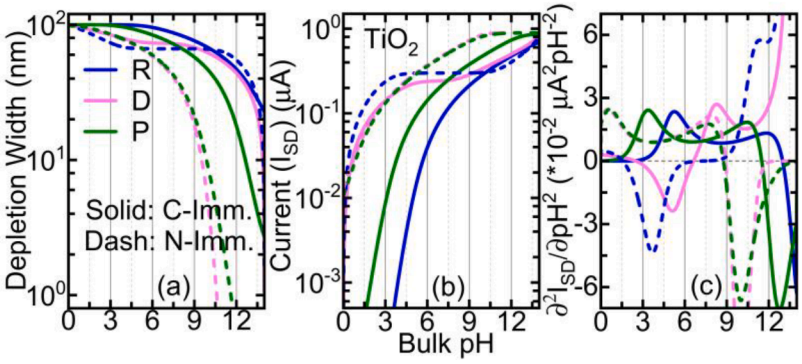

Fig. 5. (a) Depletion width (W_D) (b) drain current (I_{SD}) and (c) 2nd order derivative of I_{SD} $\left(\frac{\partial^2 I_{SD}}{\partial pH^2}\right)$ vs pH. Graphs shown are for Arginine (R), Aspartic Acid (D) & Proline (P) amino acids considering TiO_2 as a gate oxide with carboxyl group immobilised (solid line: C-Imm) and amine group immobilised (dash line: N-Imm).

form of I_{SD} and $\frac{\partial^2 I_{SD}}{\partial pH^2}$ which follows the Ψ_0 of the corresponding AAs. TiO_2 helped in generating more distinct fingerprints in terms of inflection points while maintaining the same zero-crossover points as compared to the SiO_2.

4. Conclusion

This paper presents a comprehensive analytical model that allows us to uniquely identify the signatures of different amino acids. The main parameters that are used to distinguish between the AA are the 2nd order derivative of drain current I_{SD} $\left(\frac{\partial^2 I_{SD}}{\partial pH^2}\right)$ and the surface potential Ψ_0 $\left(\frac{\partial^2 \Psi_0}{\partial pH^2}\right)$. Hence, our analytical model indeed proves the possibility of using FET-based sensors to model proteomics. More importantly, this model can provide additional information while calibrating and benchmarking the simulated results with the experimental data.

Declaration of Competing Interest

The authors declare that they have no known competing financial interests or personal relationships that could have appeared to influence the work reported in this paper.

Data availability

Data will be made available on request.

Acknowledgement

This project has received funding from the European Union's Horizon 2020 research and innovation program under grant agreement no 862539-Electromed-FET OPEN.

References

[1] The Nobel Prize in Physics 1956. NobelPrize.org. Nobel Prize Outreach AB, 2022.
[2] Bergveld P. Development of an ion-sensitive solid-state device for neurophysiological measurements. IEEE Trans Biomed Eng 1970;BME-17(1):70–1.
[3] Korri-Youssoufi H, et al. Toward bioelectronics: specific DNA recognition based on an oligonucleotide-functionalized polypyrrole. J Am Chem Soc 1997;119(31):7388–9.
[4] McGovern ME, Thompson M. Thiol functionalization of surfaces for biosensor development. Can J Chem 1999;77(10):1678–89.
[5] Syahir A, Usui K, Tomizaki K-y, Kajikawa K, Mihara H. Label and label-free detection techniques for protein microarrays. Microarrays April 2015;4(2):228–44.
[6] Rani D, Rollo S, Olthuis W, Krishnamoorthy S, Pascual García C. Combining chemical functionalization and FinFET geometry for field effect sensors as accessible technology to optimize pH sensing. Chemosensors 2021;9(2):20.
[7] van Hal REG, Eijkel JCT, Bergveld P. A general model to describe the electrostatic potential at electrolyte oxide interfaces. Adv Colloid Interface Sci 1996;69(1):31–62.
[8] Yates DE, Levine S, Healy TW. Site-binding model of the electrical double layer at the oxide/water interface. J Chem Soc, Faraday Trans 1 1974;70(0):1807.
[9] Bard AJFLR, Electrochemical methods and applications. 2000, New York; London: Wiley-Interscience.
[10] Dzombak D. 1, FFM Morel, Surface Complexation Modelling. New York: Wiley; 1990.
[11] Hiemstra T, Van Riemsdijk W. Physical chemical interpretation of primary charging behaviour of metal (hydr) oxides. Colloids Surf 1991;59:7–25.
[12] Medina-Bailon C, Kumar N, Dhar RPS, Todorova I, Lenoble D, Georgiev VP, et al. Comprehensive analytical modelling of an absolute pH sensor. Sensors 2021;21(15):5190.
[13] Dhar R, Kumar N, Pascual Garcia C, Georgiev V. Assessing the effect of scaling high-aspect-ratio ISFET with physical model interface for nano-biosensing application. Solid-State Electron 2022;195:108374.
[14] Dhar RPS, et al. TCAD Simulations of High-Aspect-Ratio Nano-biosensor for Label-Free Sensing Application. in 2021 Joint International EUROSOI Workshop and International Conference on Ultimate Integration on Silicon (EuroSOI-ULIS). 2021.
[15] Rollo S, Rani D, Leturcq R, Olthuis W, Pascual García C. High aspect ratio fin-ion sensitive field effect transistor: compromises toward better electrochemical biosensing. Nano Lett 2019;19(5):2879–87.
[16] Kosmulski M. Attempt to determine pristine points of zero charge of Nb2O5, Ta2O5, and HfO2. Langmuir 1997;13(23):6315–20.
[17] Yoon RH, Salman T, Donnay G. Predicting points of zero charge of oxides and hydroxides. J Colloid Interface Sci 1979;70(3):483–93.
[18] Rollo S, et al. High performance Fin-FET electrochemical sensor with high-k dielectric materials. Sens Actuators, B 2020;303:127215.